

1 **Land use/cover change-induced decline in terrestrial gross primary production over**
2 **the conterminous United States from 2001 to 2016**

3 Yulong Zhang^{1,2*}, Conghe Song^{1*}, Taehee Hwang³, Kimberly Novick⁴, John W. Coulston⁵,
4 James Vose⁵, Matthew P. Dannenberg⁶, Christopher R. Hakkenberg⁷, Jiafu Mao⁸, and Curtis E.
5 Woodcock⁹

6
7 ¹Department of Geography, University of North Carolina at Chapel Hill, Chapel Hill, NC, USA;

8 ²Institute for a Secure and Sustainable Environment (ISSE), University of Tennessee, Knoxville,

9 TN, USA; ³Department of Geography, Indiana University, Bloomington, IN, USA; ⁴O’Neill

10 School of Public and Environmental Affairs (SPEA), Indiana University, Bloomington, IN,

11 USA; ⁵Eastern Forest Environmental Threat Assessment Center, USDA Forest Service, Raleigh,

12 NC, USA; ⁶Department of Geographical and Sustainability Sciences, University of Iowa, Iowa

13 City, IA, USA; ⁷School of Informatics, Computing, and Cyber Systems, Northern Arizona

14 University, Flagstaff, AZ, USA; ⁸Environmental Sciences Division and Climate Change Science

15 Institute, Oak Ridge National Laboratory, Oak Ridge, TN, USA; ⁹Department of Earth and

16 Environment, Boston University, Boston, MA 02215

17
18 ***Corresponding authors:**

19 Dr. Yulong Zhang (ylzhang@utk.edu); Dr. Conghe Song (csong@email.unc.edu)

20

21

22

23

24 **Abstract**

25 As one of the most dynamic aspects of global environmental change, land use/cover change
26 (LUCC) has a profound impact on terrestrial carbon sequestration. However, LUCC-induced
27 carbon fluxes are still the most uncertain terms in global and regional carbon budgets. Ecosystem
28 gross primary production (GPP) is the total carbon uptake by vegetation through photosynthesis,
29 serving as a major control on ecosystem function and land carbon balance during and after the
30 modification of the land surface. However, accurately capturing LUCC-induced GPP changes
31 requires both high-quality land cover data and controlling for variation driven by other
32 environmental factors such as climate. In this study, we comprehensively examined the effects of
33 LUCC on annual GPP trends over the conterminous United States (CONUS) from 2001 to 2016
34 using the National Land Cover Database, a remote sensing-driven ecosystem model, and the
35 Google Earth Engine cloud computing platform. We designed a series of model experiments to
36 identify the LUCC effects on GPP by controlling climate effects. During the study period, LUCC
37 exerted a strong negative effect on total GPP across the CONUS ($[-2.2, -1.8]$ Tg C yr⁻²), while
38 climate had smaller positive effects ($[0.17, 0.92]$ Tg C yr⁻²). The LUCC-induced reduction of
39 GPP was mainly caused by net forest loss ($[-1.98, -1.39]$ Tg C yr⁻²) and urban expansion ($[-2.03,$
40 $-1.92]$ Tg C yr⁻²), but was partially offset by increases in crop area ($[+0.66, +0.79]$ Tg C yr⁻²).
41 Ensemble simulations from TRENDY did not capture the strong negative LUCC influences on
42 GPP, likely due to the deficiency of the adopted land cover data. Our study provides a novel
43 perspective on LUCC-induced GPP changes, which could help to improve our understanding of
44 ecosystem function changes and constrain the estimation of land carbon balance in the context of
45 anthropogenic activity and climate change.

46

47 **Keyword**

48 Land use/cover change (LUCC), gross primary production (GPP), National Land Cover

49 Database (NLCD), Google Earth Engine (GEE), TRENDY, CONUS

50

51 **1. Introduction**

52 Human-induced land use/cover change (LUCC) and climate change represent two of the most
53 dynamic aspects of global environmental change, which have profound impacts on land carbon
54 sequestration (Foley, 2005; Pielke, 2005; Zhang et al., 2019; Piao et al., 2020). The terrestrial
55 biosphere acts as a major carbon sink in the global carbon cycle (Falkowski et al., 2000),
56 potentially offsetting one third of fossil fuel emissions (Le Quéré et al., 2018; Friedlingstein et
57 al., 2019). However, an equivalent of about half of the total land carbon sink is reemitted back
58 into the atmosphere through LUCC, and primarily deforestation (Friedlingstein et al., 2019).
59 After fossil fuel emissions, LUCC is the second largest contributor of anthropogenic emissions to
60 the atmosphere. Nevertheless, compared to fossil fuel emissions and other components of the
61 global carbon budget, LUCC-induced carbon emissions are associated with the highest
62 uncertainty (Houghton et al., 2012; Sitch et al., 2015; Arneth et al., 2017; Friedlingstein et al.,
63 2019). Ecosystem gross primary production (GPP) is the total carbon uptake by vegetation
64 through photosynthesis (Beer et al., 2010), serving as a primary regulator on the land carbon
65 balance by offsetting potential carbon releases during and after LUCC (Hansis et al., 2015).
66 Therefore, constraining LUCC-induced GPP change could provide a better understanding of
67 ecosystem functions (Anav et al., 2015; Zhang et al., 2014, 2019) and further reduce
68 uncertainties in global and regional carbon balances (Erb et al., 2013; Arneth et al., 2017). This
69 goal is also aligned with recently renewed efforts to understand the role of LUCC in
70 implementing “natural climate solutions” (Griscom et al., 2017; Fargione et al., 2018).

71 While globally important, LUCC typically occurs locally and across various vegetation types and
72 climate zones (Sleeter et al., 2013). Precisely quantifying the influence of LUCC on GPP relies
73 on robust ecosystem models with spatially explicit land cover data, which could characterize

74 types, locations, extents and frequency of LUCC at fine spatial scales. Global or national-scale
75 LUCC-induced carbon fluxes are usually estimated in a simplified manner through bookkeeping
76 models (Coulston et al., 2015; Friedlingstein et al., 2019), relatively simple carbon accounting
77 methods based on forest inventory, agricultural statistical and/or social census data (e.g.,
78 FAOSTAT; <http://www.fao.org/faostat>). Consequently, they do not include transient responses
79 of ecosystems to environmental changes and most of them lack spatial details of LUCC
80 influences (Houghton et al., 2012; Pongratz et al., 2014; Hansis et al., 2015). Meanwhile,
81 process-based dynamic global vegetation models (DGVMs) such as TRENDY (Sitch et al.,
82 2015) have been used to quantify the LUCC effects on GPP, for example, based on century-long
83 harmonized land cover data (e.g., HYDE, LUH2) (Anav et al., 2015; Arneth et al., 2017).
84 Although DGVMs can simulate carbon dynamics with detailed biogeochemical processes, the
85 demand for sophisticated high-quality model inputs is usually hard to satisfy and their
86 operational spatial resolutions ($0.25^\circ - 1^\circ$) are usually too coarse to evaluate the effects of fine-
87 scale LUCC (Anav et al., 2015; Bastos et al., 2020). As a consequence, current bookkeeping and
88 process-based models still show large discrepancies in the estimation of LUCC-induced carbon
89 fluxes (Friedlingstein et al., 2019; Bastos et al., 2020; Harris et al., 2021).

90 Satellite observations allow near real-time, large-scale monitoring of land surface conditions
91 (Song et al., 2015), facilitating not only derivation of high frequency land cover information
92 (ESA, 2017; Sulla-Menashe et al., 2019) but also vegetation status during or after disturbances
93 (Frolking et al., 2009; Didan et al., 2015). Remote sensing driven ecosystem models, such as
94 those derived from light-use efficiency theory, provide an alternative approach for quantifying
95 fine-scale LUCC-induced GPP change (Zhang et al., 2014). Combined with fine-resolution land
96 cover datasets, such as those provided by the USGS National Land Cover Database (NLCD)

97 (Homer et al., 2020), these models have the potential to better constrain LUCC-induced changes
98 in GPP at the scale at which LUCC actually occurs (i.e., local to regional scales).

99 The conterminous United States (CONUS) possesses diverse ecosystems and heterogenous
100 landscapes, but has experienced intensive LUCCs related to anthropogenic and natural
101 disturbance over the past two decades (Homer et al., 2020). However, the patterns, magnitudes
102 and rates of LUCCs and their corresponding influences on carbon fluxes remain debatable
103 (Arneeth et al., 2017; Yu et al., 2019; Liu et al., 2020). For example, the national inventory data of
104 FAOSTAT and global harmonized land cover data (Hurtt et al., 2017) showed an increase of
105 total forest area but a decrease of cropland area over the CONUS since 2001, which contradict
106 remote sensing-based observations (Hansen et al., 2013; ESA, 2017; Li et al., 2018).
107 Accordingly, the land carbon sink over the CONUS may be largely overestimated without
108 critical fine-scale LUCC information (Liu et al., 2020) or even turned to carbon source after
109 accounting for more accurate LUCC information (Yu et al., 2019).

110 The NLCD provides more than two decades of comprehensive land cover information at a 30-m
111 spatial resolution over the CONUS (Fry et al., 2008; Yang et al., 2018). However, early versions
112 of NLCD are not quite suitable for LUCC analysis due to the data inconsistency (i.e., before and
113 after 2000), relative low cyclical update and short accumulation period (e.g., only a decade for
114 NLCD 2011 with five-year interval) (Fry et al., 2008; Homer et al., 2015). The recent release of
115 NLCD (2016) represents a next generation NLCD product with a consistent multi-temporal land
116 cover database at 2-3-year intervals since 2001 (Yang et al., 2018). Thus, the newly updated
117 NLCD provides a chance to re-evaluate the status of LUCC over the CONUS and its
118 contributions to changes in land carbon fluxes.

119 Here, we assimilated the newly released NLCD into a remote sensing-driven ecosystem model in
120 Google Earth Engine (GEE) to examine the spatiotemporal patterns of LUCC over the CONUS
121 and further isolate the effects of LUCC on annual GPP trends from climate change and
122 variability using factorial model simulations. Specifically, we addressed four scientific questions:
123 (1) What were the spatial/temporal patterns of LUCC over the CONUS from 2001 to 2016? (2)
124 How did the LUCC affect the terrestrial GPP at national/regional scales and by LUCC types? (3)
125 How different were the influences of LUCC compared to those from climate variability and
126 change? (4) To what extent did ensemble model simulations from TRENDY capture LUCC-
127 induced GPP changes identified in the analysis of the NLCD database? By answering these
128 questions, our study would offer a novel perspective on the dominant modes of LUCC-driven
129 GPP change across the CONUS, beyond which informing model predictions is also highly
130 relevant for ongoing efforts to sustain the US terrestrial carbon sink.

131

132 **2. Materials and Methods**

133 **2.1 CCW model**

134 We used the Coupled Carbon and Water (CCW) model to estimate the respective effects of
135 LUCC and climate change on GPP. CCW is a recently developed diagnostic ecosystem model
136 based on global eddy flux tower and remote sensing data (Zhang et al., 2016, 2019). In CCW,
137 GPP is estimated as the product of absorbed photosynthetically active radiation (APAR) and
138 realized LUE (\mathcal{E}) that varies with vegetation type and climate based on light-use efficiency
139 (LUE) theory:

$$140 \quad GPP = APAR \times \mathcal{E} = (PAR \times FPAR) \times \varepsilon_{pot} \times f(E) \quad (1)$$

141 where PAR is the incident photosynthetically active radiation (MJ m^{-2}), which is assumed to be

142 45% of the total short-wave radiation; FPAR is the fraction of PAR absorbed by plants, which is
 143 linearly related to remote sensing-based normalized difference vegetation index (NDVI) (Sims et
 144 al., 2005); ϵ_{pot} (g C MJ⁻¹) is the potential LUE without environmental stresses; and $f(E)$
 145 represents scalar functions that reduce LUE in responses to environmental stress. CCW accounts
 146 for environmental stress effects from diffuse radiation (R_s), temperature (T_s) and water stresses
 147 (W_s):

$$148 \quad f(E) = R_s \times T_s \times W_s \quad (2)$$

$$149 \quad R_s = 1 - K_1 \times CI \quad (3)$$

$$150 \quad T_s = \frac{(T - T_{\min}) \times (T - T_{\max})}{(T - T_{\min}) \times (T - T_{\max}) - (T - T_{\text{opt}})^2}$$

$$151 \quad (4)$$

$$152 \quad W_s = e^{-K_2 \times (VPD - VPD_{\min})} \quad (5)$$

153 where CI is a clear-sky index (defined as the ratio of actual radiation to clear-sky radiation); K_1 is
 154 a diffuse light response parameter in which a smaller K_1 indicates a stronger influence of diffuse
 155 radiation on LUE; T is the monthly mean air temperature; T_{\min} , T_{\max} and T_{opt} are the minimum,
 156 maximum and optimal air temperatures for photosynthetic activity, respectively; VPD is the
 157 monthly vapor pressure deficit (hPa); K_2 is a moisture sensitivity parameter, whereby a higher K_2
 158 indicates a larger reduction of LUE in response to VPD; and VPD_{\min} is the minimum VPD above
 159 which moisture stress starts to take effect. W_s is set to 1.0 when the VPD is lower than VPD_{\min} .

160

161 The parameters ϵ_{pot} , T_{\min} , T_{\max} , T_{opt} , K_1 , and K_2 are biome-specific (Table S1) and have been
 162 calibrated based on global flux tower data from FLUXNET2015 and remote-sensing based
 163 NDVI from MODIS-C6 (Zhang et al., 2019). Additional details about the theoretical framework
 164 and model validation at multiple levels (i.e., site-, biome- and spatial-levels) can be found in

165 previous studies (Zhang et al., 2016, 2019). Overall, CCW explained 71% of the variation in
166 tower-based GPP with a root-mean-square error of $2.0 \text{ g C m}^{-2} \text{ day}^{-1}$, which is comparable to
167 most existing remote sensing-based models of GPP (Zhang et al., 2019). In addition, the biome-
168 specific parameters, simplified yet robust model structure, and consideration of key
169 environmental constraints from temperature, water stress and light saturation all make CCW
170 particularly useful for examining the LUCC effects on GPP separately from climate change
171 effects at broad scales (Zhang et al., 2019).

172

173 **2.2 Driver datasets for CCW**

174 To drive CCW, we used all epochs of 30-m land cover data from NLCD 2016, 16-day 250-m
175 NDVI from MODIS (i.e., MOD12Q1 C6) (Didan et al., 2015), and monthly 1 km climate data
176 from Daymet3 (Thornton et al., 2017) from 2001 to 2016.

177 **2.2.1 Land cover data**

178 Based on the Landsat images and a series of ancillary land products, the United States
179 Geological Survey recently updated the 30-m NLCD to a newer version (i.e., NLCD 2016) with
180 innovative, consistent and robust methodologies (Jin et al., 2019). Different from previous
181 versions of the NLCD at 5-10 year intervals, NLCD 2016 offers multi-temporal land cover data
182 at 2-3 year intervals between 2001 and 2016 (Yang et al., 2018). The overall accuracy of 82% -
183 86% for the NLCD 2016 (Yang et al., 2018; Jin et al., 2019) outperforms existing global land
184 cover products: e.g., 73.6% for MCD12Q1 (Sulla-Menashe et al., 2019), 72-75% for ESA-CCI
185 (ESA, 2017), and 80% for GLOBELAND30 (Chen et al., 2015).

186 All seven epochs of land cover data from NLCD 2016 (i.e., 2001, 2004, 2006, 2008, 2011, 2013
187 and 2016) were utilized in this study. For those missing years, the closest land cover data were

188 used for gap-filling. The original NLCD land types were regrouped into 9 classes, including
189 evergreen forest, deciduous forest, mixed forest, shrub, grass (grassland/herbaceous and
190 pasture/hay), crop, urban, barren, and water/wetland. In this study, since we mainly focused on
191 the GPP dynamics over terrestrial ecosystems, aquatic or semi-aquatic ecosystems related to
192 water/wetlands were masked out. The remaining non-vegetated types (i.e., urban & barren) were
193 incorporated for LUCC analysis, but their GPP values were set to zero in the CCW.

194 For comparison to our NLCD 2016 analysis, we further collected annual 500-m MODIS Land
195 Cover Product (Collection 6 MCD12Q1) and annual 300-m ESA-CCI Land Cover Data for the
196 period from 2001 to 2016. We selected the classification scheme of International
197 Geosphere-Biosphere Programme (IGBP) in MCD12Q1 to compare with the NLCD 2016. The
198 ESA-CCI land cover data, which adopted a classification from the United Nations-Land Cover
199 Classification System, were converted to the IGBP in this study following (Zhang et al., 2019).
200 In addition, annual national inventory data from FAOSTAT (<http://www.fao.org/faostat/en>) and
201 0.25° Land Use Harmonization data (LUH2v2.1h) (Hurt et al., 2017) for years corresponding to
202 the study period were included for comparison to our NLCD 2016 analysis.

203

204 **2.2.2 Vegetation index data**

205 The 16-day 250-m MODIS NDVI product (i.e., MOD12Q1 C6) over the CONUS was used to
206 drive the CCW over the study period (2001-2016). The collection 6 MODIS NDVI was retrieved
207 from daily, atmosphere-corrected, bidirectional surface reflectance (Didan et al., 2015), and
208 issues of sensor degradation in the prior collection 5 were largely resolved (Zhang et al., 2017).
209 Based on the detailed Quality Control flag, poor-quality NDVI values (mostly related to clouds,
210 aerosols, snow/ice and bad geometry etc.) were linearly interpolated based on the closest good-

211 quality data within a window of 64 days. If no good quality NDVI value was found within this
212 window, the multiple-year average of high-quality 16-day values was used. Where the 16-day
213 averaged data was still unavailable, monthly averaged high-quality data was used. After the 16-
214 day smoothed series were constructed, the monthly average of NDVI was then calculated as the
215 input to the CCW.

216 **2.2.3 Climate data**

217 We obtained daily shortwave solar radiation, air temperature, and VPD from 1-km Daymet V3,
218 which was derived from in-situ meteorological observations and various supporting datasets over
219 North America (Thornton et al., 2017). We calculated VPD from daily minimum/maximum air
220 temperature and actual water vapor pressure (Allen et al., 1998). All daily variables were
221 aggregated to monthly values for model simulation. To calculate clear-sky solar radiation, we
222 adopted a 30-m DEM from GMTED2010 (Danielson & Gesch, 2011).

223 **2.2.4 Model implementation in Google Earth Engine**

224 We implemented the CCW model in Google Earth Engine (GEE), a cloud-based geospatial
225 processing platform, which has been widely used for large-scale environmental monitoring and
226 modeling (Gorelick et al., 2017; Tamiminia et al., 2020). To balance computing efficiency,
227 output storage, and input data quality, all the input data were resampled to a spatial resolution of
228 300 m. Among them, NLCD was upscaled based on the majority rule, while other data were
229 interpolated based on the nearest neighbor method.

230 **2.3 Modeling design**

231 To disentangle the effects of LUCC and climate change on GPP, we designed three groups of
232 simulation scenarios based on different combinations of model inputs (Table 1). The first group

233 (“All”) was assembled to produce the actual ensemble GPP dynamics by allowing all model
234 inputs change with time. The second group simulated LUCC effects on GPP, including two
235 simulations, S1 and S2. S1 held land cover at the initial 2001 level, but allowed all other
236 variables to change, while S2 further held FPAR at the 2001 level. We used the simulation
237 difference between All and S1 (“LUCC1”) to represent the direct effect of LUCC on GPP
238 independent of climate change effects. In CCW, land cover type determines the biome-specific
239 potential LUE and other sensitivity parameters to climate variables. However, LUCC1 did not
240 account for the potential effect of FPAR change caused by LUCC. Therefore, we further
241 considered this effect using the simulation difference between All and S2 (“LUCC2”), which
242 represents the integrated effect of LUCC. The realistic LUCC effect on GPP can be constrained
243 by LUCC1 and LUCC2. To quantify climate effects, two additional simulations (S3 and S4)
244 were conducted. S3 allowed land cover and FPAR to change but held all three climate factors
245 (solar radiation, air temperature and VPD) at the initial 2001 level, while S4 only allowed land
246 cover change with time but held all the other factors constant. The simulation difference of All –
247 S3 (“CLM1”) reflects the direct effect of climate change on GPP, while All – S4 (“CLM2”)
248 further includes the partial effect of climate change on FPAR change, and thus GPP change
249 (Table 1). Therefore, the realistic climate effect on GPP can be constrained by CLM1 and
250 CLM2.

251

252 **Table 1** Scenario designs to disaggregate LUCC and climate change effects on GPP based on
253 CCW. The symbol '▲' indicates that the input variable changes along time, while the symbol '△'
254 indicates that the input variable is fixed as the level in the initial year. The LUCC effect is
255 constrained by the direct LUCC effect from LUCC1 (i.e., All – S1) and indirect LUCC effect

256 from LUCC2 (i.e., All – S2), while climate change effect is constrained by the direct effect from
 257 CLM1 (i.e., All – S3) and indirect effect from CLM2 (i.e., All – S4).

Group	All	LUCC		Climate Change	
	-	LUCC1	LUCC2	CLM1	CLM2
	-	All – S1	All - S2	All – S3	All – S4
Simulation	All	S1	S2	S3	S4
Land Cover	▲	△	△	▲	▲
FPAR	▲	▲	△	▲	△
Radiation	▲	▲	▲	△	△
Temperature	▲	▲	▲	△	△
VPD	▲	▲	▲	△	△

258

259 2.4 Analysis methods

260 To conduct LUCC-related analyses, we first identified stable and change areas in land cover by
 261 stacking all NLCD data together. Pixels were labeled as stable areas if they did not experience
 262 change across NLCD dates. Otherwise, pixels were labeled as change areas. Any pixels
 263 classified as water or wetlands during the study period (accounting for 8% of total CONUS area)
 264 were excluded from further analysis. By comparing the initial NLCD in 2001 and the ending
 265 NLCD in 2016, a land cover transition matrix over the CONUS was calculated, and major LUCC
 266 types (including deforestation, reforestation, crop expansion, crop shrinkage, and urbanization)
 267 were identified over five sub-regions (i.e., Northwest, Midwest, Northeast, Southwest and
 268 Southeast). After that, annual GPP trends from different model simulations were analyzed and
 269 subsequent LUCC and climate change effects on GPP were assessed. It is worth noting that our
 270 LUCC study based on NLCD is only focused on the land cover change area either related to
 271 natural disturbances or anthropogenic activities. Those stable land-cover areas with land-use and
 272 management changes (e.g., change of crop types), but unidentified as changes in NLCD, were
 273 excluded in our study.

274

275 **2.5 TRENDY data**

276 To examine if land surface models capture the fine-scale LUCC-induced GPP changes identified
277 in this study, we further examined GPP simulations from TRENDY (Version 7) during the study
278 period. TRENDY contains ensemble results from multiple DGVMs and have been used to
279 quantify the effects of common historical forcing on global ecosystem dynamics (Sitch et al.,
280 2015; Quéré et al., 2018). Based on TRENDY factorial simulations, we calculated LUCC-
281 induced GPP changes based on differences between S3 (i.e., CO₂, climate and land use change
282 along time) and S2 (i.e., only CO₂ and climate change). Here we included 6 of 16 models from
283 TRENDY V7 in our analysis (Table S2) because the remaining models are not comparable with
284 the simulations in this study due to the extra modeling of nitrogen effect in S3. The spatial
285 resolutions of model outputs from TRENDY vary from $0.5 \times 0.5^\circ$ to $2 \times 2^\circ$ (Table S2). To be
286 consistent in the analysis, all TRENDY outputs were resampled to $1 \times 1^\circ$.

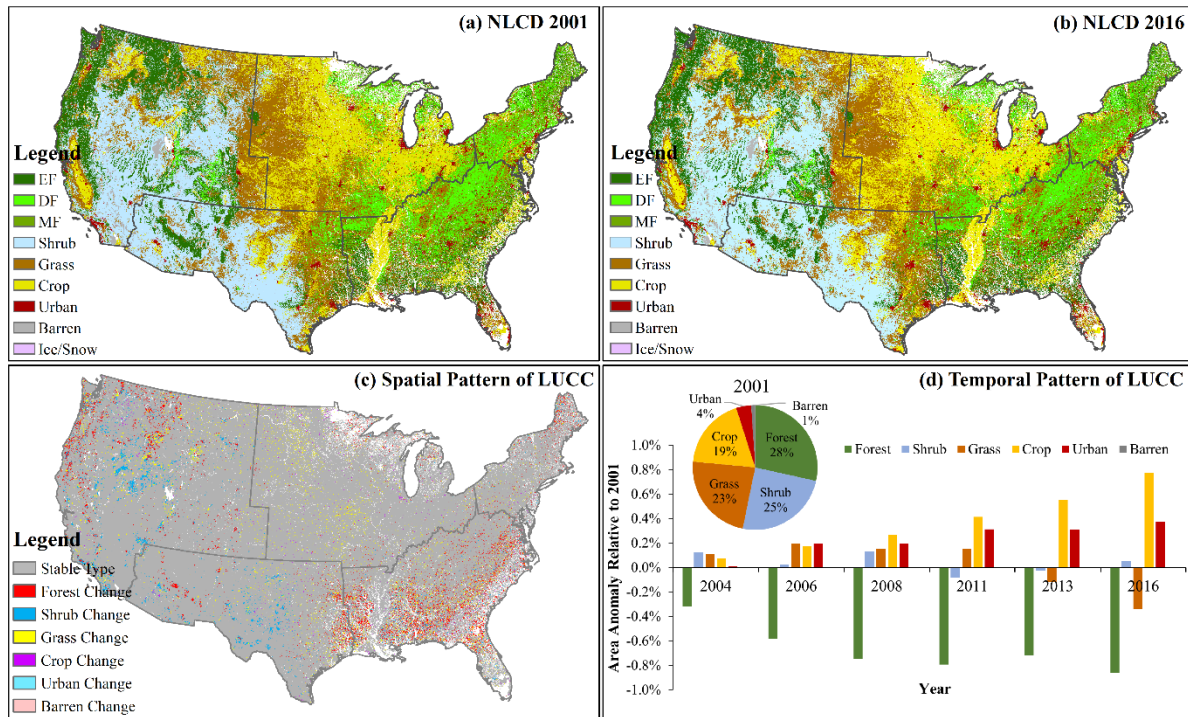
287 The LUCC data used in TRENDY V7 was from the yearly Land Use Harmonization data
288 (LUH2; version 2.1h) at a spatial resolution of $0.25 \times 0.25^\circ$ (Quéré et al., 2018). To further
289 evaluate the potential difference between TRENDY and NLCD-based simulations, we conducted
290 simulations of LUCC-induced GPP dynamics based on the fractional land use/cover state from
291 LUH2 and CCW model following the scenario Table 1. Given TRENDY accounts for land-use
292 change and management practices over the stable land-cover areas (e.g., cropland), which are
293 excluded in our study, we thus only focused on the evaluation of TRENDY and LUH2
294 simulations over the land-cover change area identified by NLCD. Due to the spatial resolution
295 difference (0.25 -degree vs 300 -m), we generated statistics in two ways: 1) aggregating the fine-
296 scale 300 -m NLCD change area mask to match the original resolution of LUH2 (0.25 -degree); 2)

297 interpolating the coarse $0.25 \times 0.25^\circ$ LUH2 simulations to 300×300 m to match the fine-scale
298 NLCD change area mask.

299 **3. Results**

300 **3.1 Spatial & temporal patterns of LUCC over the CONUS**

301 Based on all seven epochs of NLCD data, 7.9% of the total area of the CONUS (excluding
302 water/wetlands; same hereafter) experienced land cover changes at least once during the study
303 period (Fig. 1), corresponding to 567,950 km², an area larger than California. Those changes
304 primarily occurred in areas that were classified as forest (41% of total change area), grass (31%
305 of total change area) and shrubland (24% of total change area) in 2001 (Fig. 1c). From 2001 to
306 2016, forests showed the largest decrease in area (equivalent to 0.86% of the total area or 10.8%
307 of total change area), followed by grassland (4.3% of total change area) (Fig. 1d). In contrast,
308 cropland showed the largest increase in area (9.7% of total change area), followed by urban
309 (4.7% of total change area) (Fig. 1d). Shrub and barren/ice areas showed relatively small
310 changes. Note that different land cover types showed different inter-annual variabilities (Fig. 1d).
311 Overall, the changing rates of forest and urban areas tended to level off over time, while cropland
312 showed an accelerated increase.



313

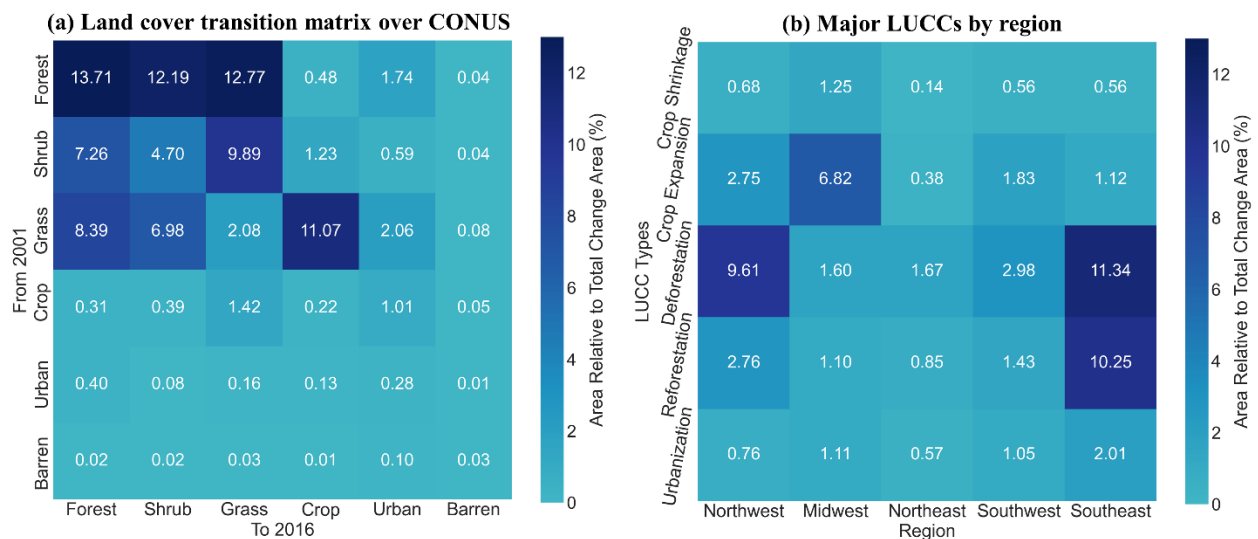
314 **Fig. 1** Spatial and temporal patterns of land use/cover change (LUCC) over the CONUS from
 315 2001 to 2016. (a) ~ (c) show spatial patterns of land cover from NLCD 2001, NLCD 2016 and
 316 LUCC between them (i.e., base year: 2001; ending year: 2016), respectively; (d) shows temporal
 317 pattern of LUCC relative to the year of 2001. All water and wetlands are masked out in (a) ~ (d).
 318 Abbreviations in (a) & (b): EF (evergreen forest), DF (deciduous forest) and MF (mixed forest);
 319 The proportion in pie chart in (d) is relative to the total area of CONUS.

320

321 From 2001 to 2016, forest losses occurred in 27.2% of the total change area, mainly transitioning
 322 to grass (12.8%) and shrub (12.2%) (Fig. 2a). Concurrently, forest gains were observed in 16.4%
 323 of the change area, largely converted from grass (8.4%) and shrub (7.3%). Although net
 324 shrubland change was small (0.7%), it had large gross gains (19.7%) and losses (19.0%), mostly
 325 related to grass and forest conversions (Fig. 2a). During this period, only 3.2% of the total

326 change area showed crop losses, but 12.9% of the total change area exhibited crop gains, mainly
 327 at the expense of grass (Fig. 2a). Similarly, urban losses represented a very small fraction (0.8%)
 328 of the total change area, but urban gains from forest and grass were relatively large (4.7%).
 329 Interestingly, all land covers showed a certain portion in the disturbed area (0.03% ~ 13.7% of
 330 the total change area), which indicate each land-use/land-cover class has at least one disturbance
 331 event within the study period. At the regional scale, both forest losses and forest gains were
 332 mainly located in Southeast and Northwest (Fig. 2b). Crop expansion and urbanization were
 333 mainly found in the Midwest and Southeast, respectively (Fig. 2b).

334



335

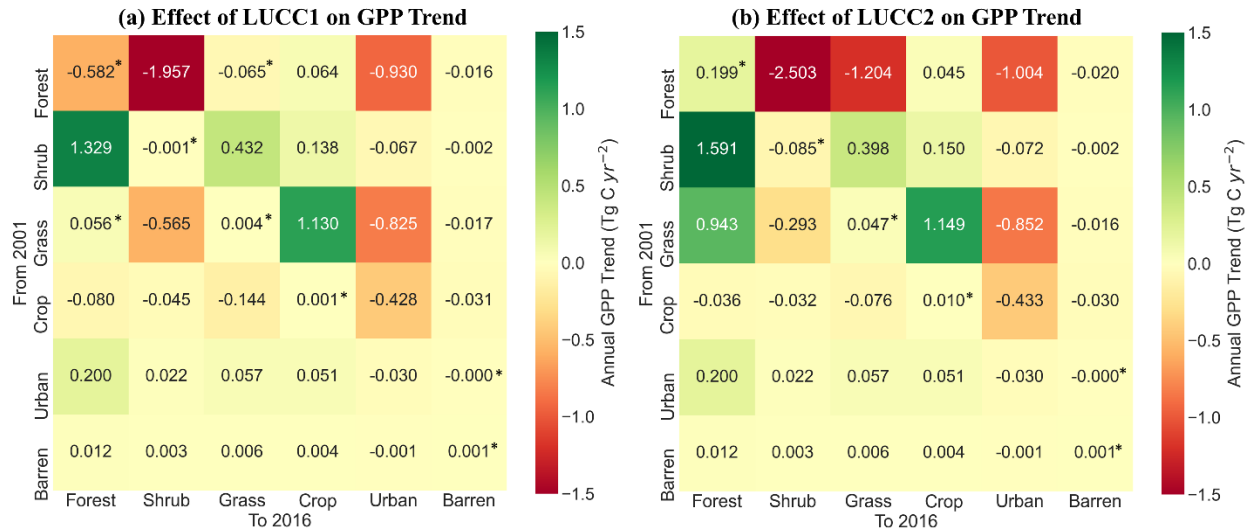
336 **Fig. 2** Land cover transition matrix over the CONUS (a) and major LUCCs by regions (b) from
 337 2001 to 2016. Numbers in (a) and (b) represent proportions of total change area.

338

339 **3.2 Effects of LUCC on GPP across LUCC types**

340 We evaluated the effects of LUCC, independent of climate effects, on the annual GPP trends
341 using the LUCC1 (accounting for direct land cover change) and LUCC2 (further accounting for
342 LUCC-induced canopy function change) model simulations (Table 1; Fig. 3). Over the CONUS,
343 forest losses exerted a strong negative effect on GPP (i.e., [-4.69, -2.90] Tg C yr⁻²; range given
344 by LUCC1 and LUCC2, same hereafter), primarily due to the conversions to shrub ([-2.50, -
345 1.96] Tg C yr⁻²), grass ([-1.20, -0.07] Tg C yr⁻²) and urban ([-1.00, -0.93] Tg C yr⁻²) classes. On
346 the other hand, forest gains mainly from shrub and grass conversion resulted in a positive GPP
347 effect (i.e., [1.52, 2.71] Tg C yr⁻²). Together, net forest change had a significant negative effect
348 on GPP (i.e., [-1.98, -1.39] Tg C yr⁻²).

349 Urban expansion exerted a strong and consistent negative effect on GPP regardless of which type
350 of vegetation was replaced, especially for forest ([-1.00, -0.93] Tg C yr⁻²), grass ([-0.85, -0.83]
351 Tg C yr⁻²) and cropland ([-0.43, -0.43] Tg C yr⁻²) (Fig. 3). Since there was very little loss of
352 urban area, the cumulative net effect of urban change on GPP was even stronger ([-2.03, -1.92]
353 Tg C yr⁻²) than the net effect of forest change. Crop expansion had a positive effect on GPP
354 ([+1.39, +1.40] Tg C yr⁻²), mostly from replacement of grass cover (Fig. 3). Overall, the net
355 effect of crop change on GPP was [+0.66, +0.79] Tg C yr⁻² after considering the negative GPP
356 effect from crop shrinkage. All stable land covers with occasional disturbances showed
357 nonsignificant GPP trends during the study period (i.e., $P > 0.05$; Fig. 3), which were not
358 involved in the above integration analysis.



359

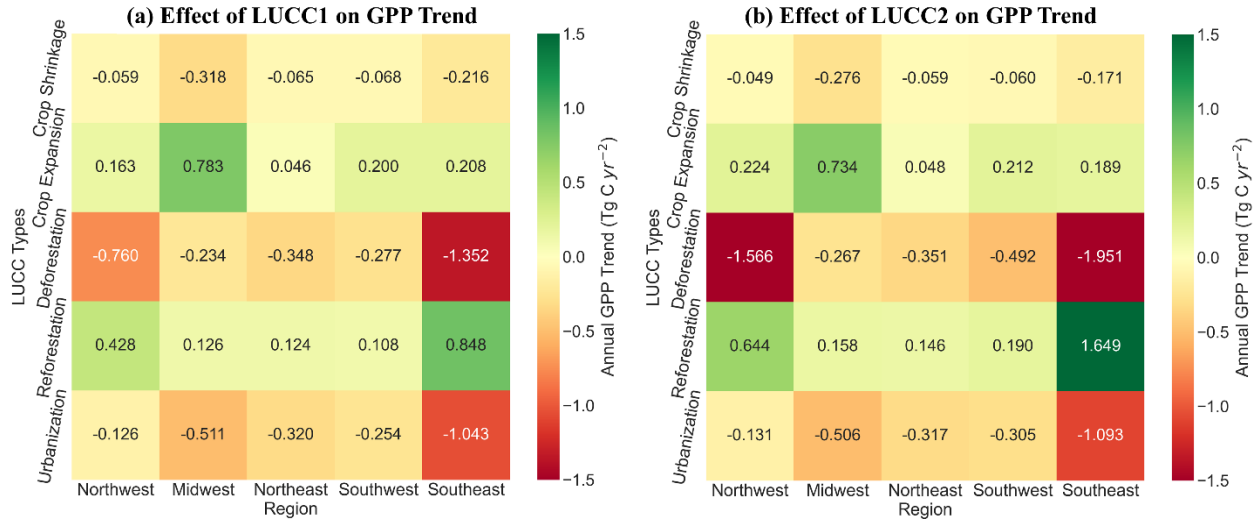
360 **Fig. 3** Effects of LUCC on annual GPP trends across LUCC types constrained by simulations
 361 of LUCC1 (a) and LUCC2 (b). Model simulations of LUCC1 and LUCC2 are seen in Table

362 1. All GPP trends are statistically significant (i.e., $P < 0.05$) unless labeled by *.

363

364 3.3 Effects of major LUCC types on GPP by regions

365 At the regional scale, forest loss (or deforestation) contributed to the largest GPP reductions in
 366 the Southeast ($[-1.95, -1.35]$ Tg C yr⁻²) and Northwest ($[-1.57, -0.76]$ Tg C yr⁻²) (Fig. 4) while
 367 forest gain (or reforestation) contributed only minor GPP increases in the same two regions,
 368 leading to large net negative effects of forest LUCC on GPP in both regions. Urbanization
 369 resulted in strong GPP reductions mainly in the Southeast ($[-1.04, -1.09]$ Tg C yr⁻²) and Midwest
 370 ($[-0.51, -0.51]$ Tg C yr⁻²). Crop expansion enhanced annual GPP trends in all regions, especially
 371 in the Midwest ($[0.73, 0.78]$ Tg C yr⁻²). However, the Midwest was also the region with the
 372 largest negative GPP effect due to cropland shrinkage ($[-0.32, -0.28]$ Tg C yr⁻²) (Fig. 4).



373

374

Fig. 4 Effects of major LUCC types on annual GPP trends across regions constrained by simulations of LUCC1 (a) and LUCC2 (b). Model simulations of LUCC1 and LUCC2 are seen in Table 1. All GPP trends here are statistically significant (i.e., $P < 0.05$).

375

376

377

378 3.4 Comparison of LUCC effect with climate effect on GPP

379

Annual total GPP over the change area of CONUS showed a large inter-annual variation from

380

2001 to 2016 (Fig. 5a). Our simulations indicated that LUCC explained 22.8% ($P < 0.01$;

381

LUCC1) to 43.2% ($P < 0.01$; LUCC2) of this variation, which is much smaller than climate

382

effects (i.e., 70.5 % ($P < 0.01$; CLM2) to 73.1% ($P < 0.01$; CLM1)) (Fig. 5a). However, for the

383

long-term GPP trend, LUCC exerted a significant negative effect of $-2.22 \text{ Tg C yr}^{-2}$ ($P < 0.01$;

384

LUCC1) to $-1.83 \text{ Tg C yr}^{-2}$ ($P < 0.01$; LUCC2) (Fig. 5b). In contrast, climate change played a

385

minor role in driving the GPP trend, with positive (but not statistically significant) effects of 0.17

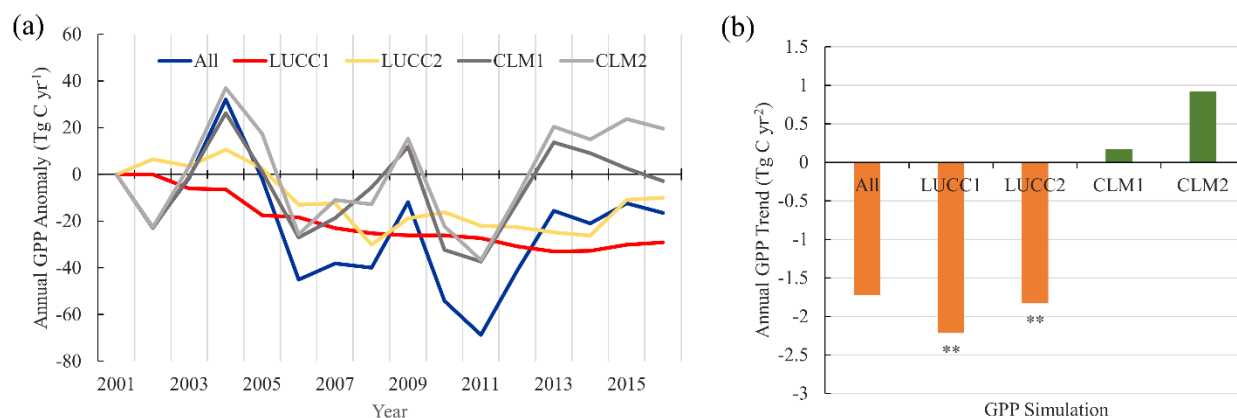
386

Tg C yr^{-2} ($P > 0.05$; CLM1) to $0.92 \text{ Tg C yr}^{-2}$ ($P > 0.05$; CLM2) (Fig. 5b). Overall, the actual

387

GPP over the change area decreased during the study period ($-1.72 \text{ Tg C yr}^{-2}$, $P = 0.21$), though

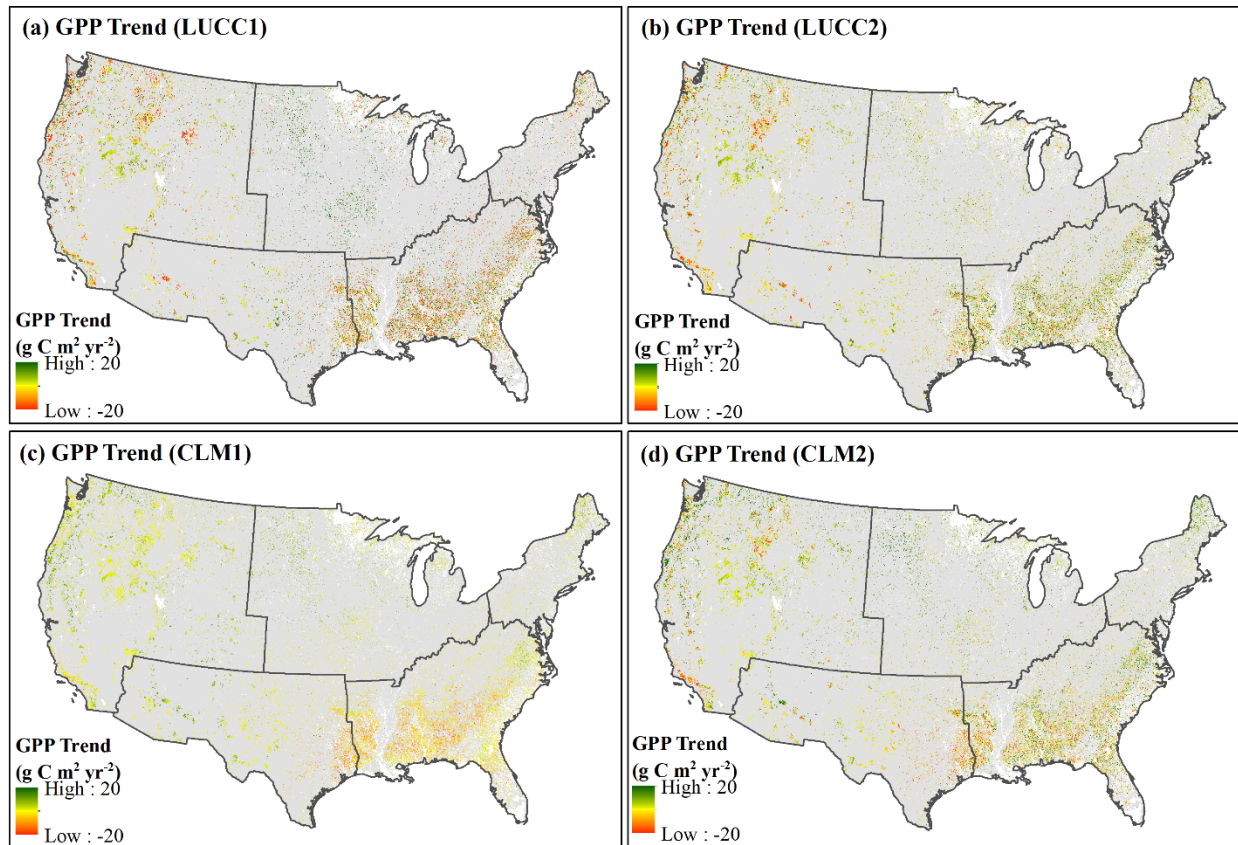
388 the trend was not statistically significant due to the high interannual variability of GPP and since
389 the LUCC effects on GPP were partially mitigated by climate change effects.



390
391 **Fig. 5** Effects of land use/cover change (LUCC) and climate change on interannual variations (a)
392 and trends (b) in total GPP over change areas across CONUS. The anomaly in (a) is relative to
393 the base year of 2001. Model simulations (i.e., LUCC1, LUCC2, CLM1 and CLM2) are seen in
394 Section 2 and Table 1. The label ** in (b) represents the significance level of annual trend (i.e., P
395 < 0.01).

396
397 In most regions (except the Midwest), LUCC effects on GPP trends were stronger and more
398 negative than climate effects over the change areas (Figs. 6 & 7). The statistically significant
399 area (i.e., P < 0.05) for LUCC effects on GPP (i.e., 51.1% of total change area for LUCC2 and
400 65.7% for LUCC1) is much larger than that for climate effects (i.e., 10.6% for CLM1 and 25.8%
401 for CLM2) (Fig. S3). In the Midwest, LUCC showed an overall positive GPP effect mainly due
402 to cropland expansion (Figs. 4 & 7). The weak positive climate effect further enhanced the GPP
403 increase over this region. Besides the Midwest, the significant negative LUCC effect on GPP in
404 the Northwest and Northeast were also to some degree eased by weak positive climate effects

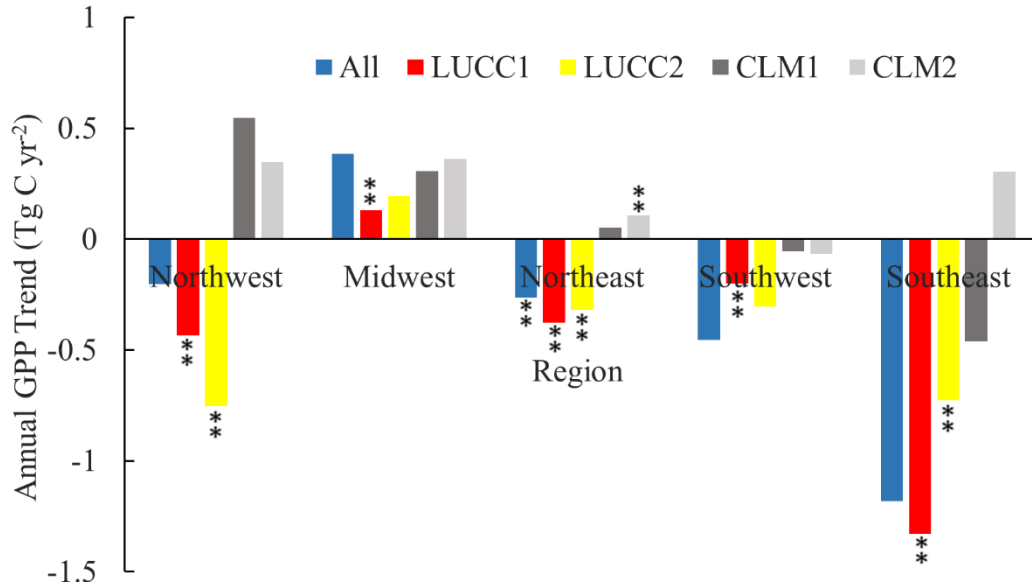
405 (Fig. 7). However, in the Southeast and Southwest, weak negative climate effects slightly
406 reinforced negative LUCC effects on GPP.



407
408 **Fig. 6** Spatial patterns of effects of LUCC (a, b) and climate change (c, d) on annual GPP trends
409 from 2001 to 2016 over change areas across CONUS, with stable areas (gray), and water/wetland
410 areas (white). Model simulations (i.e., LUCC1, LUCC2, CLM1 and CLM2) are described in
411 Section 2 and Table 1, and corresponding statistical significances are shown in Fig. S3.

412

413



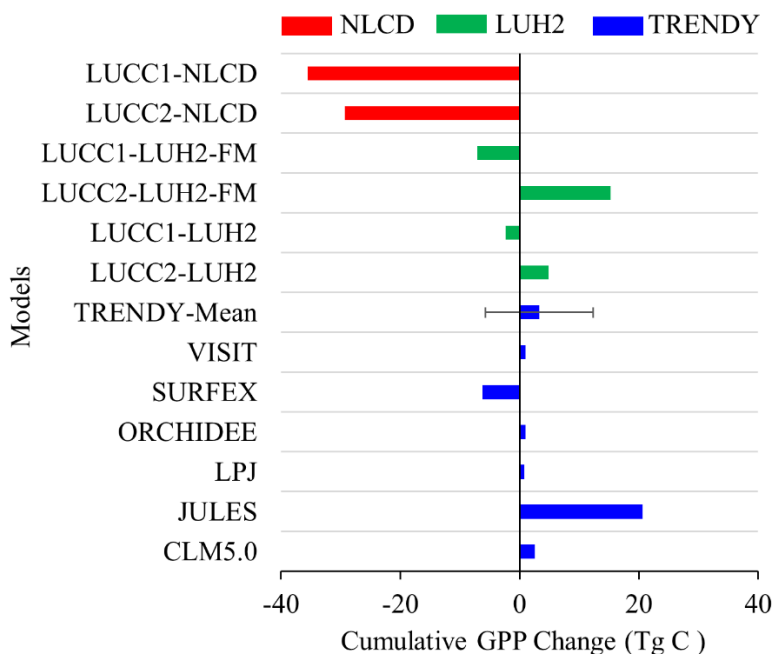
414

415 **Fig. 7** Effects of LUCC and climate change on annual total GPP trends over change areas of
 416 different regions in CONUS. The label ** represents the statistical significance level of annual
 417 GPP trend (i.e., $P < 0.05$).

418 3.5 Evaluation of LUCC effects on GPP from the TRENDY ensemble

419 During the study period, the TRENDY model ensemble showed a contrasting LUCC effect on
 420 GPP compared to CCW (Fig. 8). According to CCW, LUCC had a strong negative effect on
 421 annual GPP, with a cumulative change in the range of $[-42.3, -30.3]$ Tg C from 2001 to 2016.
 422 However, in ensemble simulations from TRENDY, LUCC had a weak positive influence on
 423 GPP, with a cumulative GPP change of 3.9 ± 9.0 Tg C over the change area. Among TRENDY
 424 models, 5 of 6 showed positive LUCC influences with the maximum GPP effect of 20.6 Tg C
 425 from JULES (Fig. 8), while the SURFEX model showed a negative influence (i.e., -6.2 Tg C).
 426 However, the latter is still out of the value range suggested by the CCW. Our independent
 427 simulations based on LUH2 showed similar LUCC effect on GPP with a range of $[-2.4, 4.9]$ Tg
 428 C based on the coarse NLCD change mask (i.e., 0.25-degree) and a slightly wider range of $[-7.1,$

429 15.3] Tg C based on the fine-scale change mask (i.e., 300-m). Despite differences from these two
 430 statistical masks, simulated GPP influences from LUH2 based on CCW are comparable with
 431 TRENDY ensemble means, suggesting the deficiency of LUH2 may be likely responsible for the
 432 underestimation of LUCC-induced negative GPP influences in TRENDY.



433
 434 **Fig. 8** Comparisons of LUCC-induced GPP changes from NLCD, LUH2 and TRENDY over the
 435 change area identified by NLCD from 2001 to 2016. LUCC-induced GPP trends from NLCD
 436 and LUH2 were simulated by CCW and based on model scenarios of LUCC1 and LUCC2 in
 437 Table 1, while LUCC influences from all TRENDY models were the differences between S3 and
 438 S2 in Table S2. Note that LUCC1-NLCD, LUCC2-NLCD, LUCC1-LUH2-FM and LUCC2-
 439 LUH2-FM were derived based on the fine-scale land-cover change mask (i.e., 300-m), while
 440 other simulations based on the masks with their original coarse spatial resolutions. Annual GPP
 441 anomalies for all these model simulations are shown in Fig. S2.

442 **4. Discussion**

443 **4.1 Spatial & temporal patterns of LUCC**

444 Our study highlighted the major patterns of LUCC over the CONUS based on the most recent
445 NLCD dataset. Excluding changes in water and other wetlands, LUCC occurred over 7.9% of the
446 total CONUS area from 2001 to 2016 (Fig. 1), which was mainly characterized by forest loss
447 (10.8% of total change area), crop expansion (9.7% of total change area), and urbanization (4.7%
448 of total change area) (Fig. 2). Currently, debates still exist on the major patterns of LUCC over
449 the CONUS. For example, the national inventory data from FAOSTAT shows an increasing
450 trend in total forest area, but a decreasing trend in cropland over the CONUS since 2001 (Fig.
451 S3). The commonly used global harmonized land cover data of LUH2, with a spatial resolution
452 of 0.25 degree and constrained by FAOSTAT, shows similar forest and cropland trends despite
453 more inter-annual fluctuation (Fig. S3). Conversely, remote-sensing based global land cover
454 products such as MODIS (500-m resolution) and ESA-CCI (300-m resolution) show a decrease
455 in forest areas, but no trend or even an increase in croplands (Fig. S3). Our study, based on the
456 up-to-date NLCD with a nominal resolution of 30 m, could help to assess the differences and
457 potentially reconcile the debate on the recent LUCC pattern over the CONUS.

458
459 Overall, opposite LUCC trends of FAOSTAT/LUH2 with NLCD 2016 reflect the deficiency of
460 these two data sources in characterizing regional LUCC signals (Goldewijk et al., 2017; Yu et
461 al., 2019). The coarse spatial resolution of LUH2 or incomplete spatial representation of
462 FAOSTAT may not well document LUCC predominantly occurring at a finer, more localized
463 scale. Another possible reason is that FAOSTAT/LUH2 focus on the information of land use,
464 while NLCD mainly on the land cover. The difference in land use- and cover- definitions here
465 contributed to the discrepancies (Coulston et al., 2014). For example, timber harvest will not

466 change the land use type of the area as long as the land is not converted to be used for some other
467 purposes (e.g., agriculture). The deforested area, in contrast, is likely to be identified as non-
468 forest after the harvest based on remotely sensed data. Therefore, a fair portion of forest losses
469 by timber harvest as well as other natural disturbances that are documented in NLCD may be
470 missing in FAO/LUH2. In addition, based on an independent high-resolution multisource
471 harmonized national LUCC database over the CONUS, Yu et al. (2019) found a striking
472 underestimation of cropland changes in LUH2. Such underestimation was mainly inherited from
473 the national inventory data from FAOSTAT, which largely underestimated crop expansion due
474 to its cropland definition, and this uncertainty of cropland change was further propagated to the
475 modeled forest change in LUH2 (Goldewijk et al., 2017; Yu et al., 2019). Remote sensing-based
476 global land cover products were more consistent with NLCD 2016 than FAOSTAT/LUH2, but
477 the MODIS land cover product showed higher biases in absolute areas for different land covers,
478 especially for forests and shrublands, while ESA-CCI showed less interannual variation than
479 NLCD 2016 (Fig. S3). Such discrepancies could result from differences in land cover/type
480 definition, classification strategies, and remote sensing data with varying spatial/temporal
481 resolutions and spectral characteristics (Li et al., 2018; Sulla-Menashe et al., 2019).

482

483 The NLCD 2016 revealed several key characteristics of LUCC across the CONUS. For example,
484 forest loss was mainly associated with conversion to grass and shrubland during the study period
485 (Fig. 2), which differs from tropical deforestation that is mainly linked to cropland expansion
486 (Barracough, 2013; Pendrill et al., 2019). The Southeast and Northwest are the two major
487 regions affected by deforestation in the CONUS (Fig. 2), which were largely driven by timber
488 harvesting, fire and mortality from drought and insect outbreaks (Williams et al., 2010; Curtis et

489 al., 2018; Howard & Liang, 2019; Homer et al., 2020). Cropland expansion mostly occurred at
490 the expense of grassland, mostly in the Midwest, which is consistent with previous research
491 (Wright & Wimberly, 2013; Yu & Lu, 2018). Urbanization, occurring most prominently in the
492 Southeast, was largely linked to grassland and forest losses (Fig. 2). These transitions differed
493 from other countries with urbanization mainly at the cost of cropland (d'Amour et al., 2017; van
494 Vliet et al., 2017). During the study period, the rate of forest loss tended to slow down after 2011
495 (Fig. 1d), generally consistent with national industrial timber markets (Howard & Liang, 2019;
496 Homer et al., 2020). A similar temporal pattern was also observed for urbanization (Fig. 1d),
497 which was possibly linked to the 2008 global economic recession (Homer et al., 2020).

498

499 **4.2 Decoupling effects of LUCC on GPP from climate change**

500 LUCC induced by anthropogenic activity and natural disturbances have profound impacts on
501 terrestrial GPP. However, such influences are usually aggregated with other environmental
502 factors, such as climate, and empirically disentangling their effects is still a challenge. In this
503 study, we decoupled the effects of LUCC and climate change on terrestrial carbon sequestration
504 based on a remote sensing-based ecosystem model and newly released high-quality land cover
505 data. Through designed model simulations, we narrowed down the effect of LUCC on recent
506 GPP changes over the CONUS to a specific range on the top of the influence of climate
507 change/variability.

508

509 From 2001-2016, we observed a strong negative effect on GPP from deforestation in the
510 CONUS (i.e., [-4.69, -2.90] Tg C yr⁻²), especially in the Southeast ([-1.95, -1.35] Tg C yr⁻²) and
511 Northwest ([-1.57, -0.76] Tg C yr⁻²). Although reforestation positively affected GPP (i.e., [1.52,

512 2.71] Tg C yr⁻²), it did not completely offset the negative effects of deforestation, resulting in an
513 overall net negative GPP trend by forest cover change over the CONUS (Figs. 3 & 4). Forests
514 are the key biome in maintaining ecosystem functions and serve as a major contributor in land
515 carbon sequestration (Domke et al., 2020; Woodbury et al., 2007). Previous studies in China
516 showed that the national-scale forest afforestation/reforestation programs since 2000 have
517 promoted substantial vegetation productivity (Zhang et al., 2014; Chen et al., 2021). Here, the
518 contrasting picture over the CONUS revealed a worrisome trend on the recent decline of GPP
519 related to forest change. Depending on the specific mechanisms driving deforestation in different
520 regions (e.g., Southeast mainly related to timber harvest and Northwest mainly related to fire)
521 (Harris et al., 2016; Curtis et al., 2018), active forest management—such as fire suppression,
522 timber harvest control, shifting to non-timber forest products or tree planting—could be useful in
523 mitigating the negative effects on GPP from forest change (Noormets et al., 2015; Domke et al.,
524 2020). However, some federal forest management rules may not be applicable to privately-
525 owned forests. For example, the forests in the Southeast is predominantly privately owned (Wear
526 & Greis, 2002), the timber harvesting contributed significantly to deforestation in this region.
527

528 Compared with forests, urbanization affected a much smaller area (Fig. 2), but the net effects on
529 GPP were disproportionately high ([-2.03, -1.92] Tg C yr⁻²), even stronger than net forest cover
530 changes due to the cumulative and direct effects of removing all vegetation (Fig. 3). The
531 Southeast ([-1.04, -1.09] Tg C yr⁻²) and Midwest ([-0.51, -0.51] Tg C yr⁻²) were the two major
532 regions associated with strong GPP reductions caused by urbanization (Fig. 3). Our findings on
533 the substantial effect of urbanization on GPP is generally consistent with previous vegetation
534 productivity studies (Liu et al., 2019; Li et al., 2020). However, due to the treatment of urban

535 areas as a homogenous surface without plants, the impact of urbanization on GPP in our study
536 may be overestimated (Guan et al., 2019).

537

538 Unlike forest and urban changes, the net change in croplands showed an overall positive effect
539 on GPP (i.e., [+0.66, +0.79] Tg C yr⁻²). Crop expansion occurring primarily at the cost of
540 grasslands was a major contributor to GPP ([+1.39, +1.40] Tg C yr⁻²) over the study period. Due
541 to crop expansion, the Midwest became the only region with an overall positive LUCC effect on
542 GPP (Figs. 6 & 7). Croplands tend to be more productive than other natural vegetation (e.g.,
543 grasslands) due to human management (e.g., irrigation, fertilization, selection of productive
544 cultivars; Licker et al., 2010), resulting in a positive net effect on GPP. However, due to the
545 exceptionally high turnover rate of carbon in crop systems (e.g., linked with harvest and
546 consumption), cropland has limited potential in carbon storage when compared with natural
547 vegetation (Wolf et al., 2015). Therefore, crop expansion, even if it increases GPP and net
548 primary production, would likely have less effect on the land carbon sink, and thus less potential
549 to mitigate the ongoing global warming (Bajželj et al., 2014; Zhang et al., 2019). In addition,
550 widespread crop expansion in the Midwest at the cost of grasslands has threatened biodiversity in
551 this region (Wright & Wimberly, 2013; Lark et al., 2015, 2020).

552

553 Altogether, our study shows a strong negative influence of LUCC on annual GPP over the
554 CONUS (i.e., [-2.6, -1.9] Tg C yr⁻²), which outweighed the slight positive GPP trends from
555 climate (i.e., [0.17, 0.92] Tg C yr⁻²). However, climate did play a major role in determining inter-
556 annual variation of GPP over the change area (Fig. 5). Theoretically, the influence of LUCC on
557 GPP will diminish or even flatten with time due to post-disturbance recovery/succession

558 (Lambin et al., 2001; Wang et al., 2020). During this period, climate will either enhance or delay
559 this process along with other environmental and human factors. In this study, we showed the
560 spatial pattern of climate influences on GPP by overlaying the effect of LUCC (Figs. 6 & 7).
561 Overall, climate change/variability alleviated negative LUCC effects in the northern CONUS but
562 worsened their effects in the southern CONUS (Fig. 6) largely due to droughts (Berdanier &
563 Clark, 2016; Park Williams et al., 2017). Our efforts in decoupling the effects of LUCC and
564 climate change on GPP can help enhance our understanding of recent carbon dynamics related to
565 human and natural disturbances over the CONUS.

566

567 **4.3 Performance of TRENDY ensemble simulations**

568 Based on the long-term LUH2 global harmonized land use data, land surface models from the
569 TRENDY ensemble provide estimates of the influence of LUCC at both the global and regional
570 scales (Sitch et al., 2015; Quéré et al., 2018;). However, our evaluation showed that none of the
571 selected models captured the strong negative GPP effects over the CONUS (Fig. 8). On the
572 contrary, 5 of 6 models simulated even positive LUCC effects on GPP. Our simulations based on
573 CCW (Fig. 8) further suggested that these discrepancies were likely caused by the uncertainty in
574 the LUH2 dataset (Goldewijk et al., 2017; Yu et al., 2019), which shows opposite trends of forest
575 and cropland areas over the CONUS when compared with the finer-resolution remote sensing
576 products (Fig. S3). Previous studies indicated that carbon emissions from LUCC over the
577 CONUS have been largely underestimated due to the mischaracterization of crop and forest
578 changes (Yu & Lu, 2018; Yu et al., 2019). Our study suggests that ignoring the strong GPP
579 reductions caused by LUCC might be a key reason for the overestimation of land carbon sink
580 over the CONUS (Liu et al., 2020). Given that TRENDY ensemble simulations provide much of

581 the basis for the Global Carbon Budget (Quéré et al., 2018; Friedlingstein et al., 2019), which
582 shows large uncertainties in LUCC-induced carbon flux, our study provides evidence for a
583 source of uncertainties in global carbon balance, to which much more attention needs to be paid.
584 However, it is worth noting that discrepancies between TRENDY and our CCW simulations are
585 further related to other potential factors such as model structures (process-based models for
586 TRENDY vs light-use efficiency model for CCW), model implementations for LUCC effect
587 (focus of land-use change and management practices for TRENDY vs land cover change for
588 CCW), and differences from climate inputs (global climate data for TRENDY vs regional
589 climate data for CCW) (Bastos et al. 2020). These aspects are not strictly quantified in our study,
590 but worthy of future investigation.

591

592 **4.4 Implications & uncertainties**

593 Reducing anthropogenic carbon emissions is a critical mechanism for mitigating global warming
594 below a secure threshold, which is an urgent yet challenging task (Rogelj et al., 2016). The
595 actions through conservation, restoration and improved land management are the cost-effective
596 ways or “natural climate solutions” to global warming mitigation (Griscom et al., 2017).
597 Currently, a series of “natural climate solutions” on natural and agricultural lands are evaluated
598 to sustain the U.S. terrestrial carbon sink and meet Paris Agreement carbon targets (Fargione et
599 al., 2018). Among them, reforestation, natural forest management and preservation of grassland
600 show the highest climate mitigation potential (Fargione et al., 2018). However, according to our
601 study based on the newest NLCD database, the recent LUCC trend since 2001 (characterized by
602 net forest loss, cropland expansion from grassland, and urban expansion from forest and
603 grassland; Fig. 2) appears to departure from these initiatives. How to account for the past LUCC

604 trajectory and the weakened carbon sequestration capacity identified by this study is critical in
605 implementing the ongoing natural climate solutions (Roe et al., 2019; Anderegg et al., 2020).

606 In this study, we comprehensively examined the spatially detailed and regionally aggregated
607 LUCCs and their impacts on vegetation productivity over the CONUS. Currently, it is still a
608 challenge to effectively disaggregate LUCC effect on GPP from climate change/variability
609 effect. Based on a remote sensing-driven ecosystem model and scenario simulations, we teased
610 out the respective effect of LUCC and climate change on GPP in specific ranges rather a definite
611 quantity, which we believe to be more reasonable than previous modeling studies (Zhang et al.,
612 2014; Sun et al., 2018). However, it is worth noting that simulations for LUCC (i.e., LUCC2)
613 and climate (i.e., CLM2) alone may have confounding effects from each other and potentially
614 other factors (e.g., regrowth, CO₂ fertilization, land management etc.) that confounded the signal
615 of canopy greenness, which are hard to separate under our current modeling scheme. Combining
616 our remote-sensing constrained estimations and process-based models with localized high-
617 quality LUCC inputs is a promising way to better understand LUCC-induced carbon dynamics.

618 In addition, the biome of wetland was excluded in our study given our focus on terrestrial
619 ecosystems. Although total wetlands increased over a relatively small area (i.e., 0.09% of total
620 CONUS area) (Homer et al., 2020), conversions between wetlands and other vegetation types,
621 and among wetlands themselves (e.g., herbaceous vs. woody) may still exert a significant GPP
622 control, which is worthy of future exploration. Third, our study focused on a relatively short
623 period from 2001 to 2016 due to temporal constraint of the NLCD records. With more updates of
624 historic and recent NLCD in the future, LUCC influences on GPP could be further refined and
625 re-evaluated. Lastly, our study is focused on GPP, a primary control on the net carbon exchange
626 (NEE). However, NEE is further constrained by ecosystem respiration (i.e., autotrophic and

627 heterotrophic) (Chapin et al., 2006). How LUCC influences the ecosystem respiration and net
628 land carbon balance over the CONUS is an interesting topic, which is worthy of exploration in
629 the future.

630

631 **5. Conclusions**

632 Based on NLCD 2016 and a remote-sensing driven ecosystem model on the GEE cloud platform,
633 we explored the effect of LUCC on GPP over the conterminous U.S. from 2001 to 2016. During
634 the study period, forest loss, cropland expansion, and urbanization dominated LUCC patterns.
635 Our model simulations estimated the net effect of forest changes on total GPP was [-1.98, -1.39]
636 Tg C yr⁻², followed by urban change ([-2.03, -1.92] Tg C yr⁻²) and crop change ([+0.66, +0.79]
637 Tg C yr⁻²). Regionally, the Southeast contributed the largest GPP reduction due to deforestation
638 (-1.95, -1.35] Tg C yr⁻²), followed by the Northwest ([-1.57, -0.76] Tg C yr⁻²), while Midwest
639 contributed largest GPP increase related to crop expansion ([0.73, 0.78] Tg C yr⁻²), and Southeast
640 contributed the largest GPP reduction related to urbanization ([-1.0, -1.1] Tg C yr⁻²). Overall,
641 LUCC led to a strong negative trend on total GPP over the CONUS ([-2.2, -1.8] Tg C yr⁻²), while
642 climate change had a relatively small positive effect (but not statistically significant) over the
643 LUCC area ([0.17, 0.92] Tg yr⁻¹) during the study period. Ensemble simulations from TRENDY
644 did not capture the strong negative effects of LUCC on GPP, likely due to the coarse spatial
645 resolution LUCC dataset used. Our study demonstrates that recent LUCC appears to reduce the
646 carbon sequestration capacity of the land surface across the CONUS in ways that not particularly
647 well represented in land surface models. Such a novel perspective on LUCC-induced GPP
648 changes could enhance our understanding of ecosystem function changes and carbon dynamics
649 under the background of anthropogenic activity and climate change.

650

651 **Acknowledgements**

652 We acknowledge USGS for providing NLCD 2016 data, NASA Science Teams for providing
653 MODIS VI products and Daymet3 climate data, the Dynamic Global Vegetation Model Project
654 team for providing TRENDY V7 data, and Earth Engine platform provided by Google. This
655 study is supported by NASA Carbon Cycle Science (NNX17AE69G). J. Mao was supported by
656 the Terrestrial Ecosystem Science Scientific Focus Area (TESSFA) project funded by the US
657 Department of Energy, Office of Science, Office of Biological and Environmental Research. Oak
658 Ridge National Laboratory is managed by UT-Battelle, LLC, for the DOE under contract DE-
659 AC05-100-00OR22725. The authors declare no conflict of interests.

660

661 **Supplementary Information**

662 **Table S1.** Biome-specific parameters of the CCW used in this study.

663 **Table S2.** Selected models from TRENDY V7

664 **Fig. S1** Statistical significance levels for annual GPP trends regulated by the effects of LUCC (a,
665 b) and climate change (c, d) from 2001 to 2016 over change area of CONUS

666 **Fig. S2** Comparisons of LUCC-induced annual GPP anomalies from TRENDY (a), LUH2 and
667 NLCD (b) over the change area identified by NLCD from 2001 to 2016

668 **Fig. S3** Evaluations of major land cover changes from national inventory data of FAOSTAT,
669 LUH2, ESA-CCI and MODIS-C6 data based on NLCD

670

671 **References**

- 672 Allen, R. G., Pereira, L. S., Raes, D., & Smith, M. (1998). Crop evapotranspiration-Guidelines
673 for computing crop water requirements-FAO Irrigation and drainage paper 56. *Fao, Rome*,
674 300(9), D05109.
- 675 Anav, A., Friedlingstein, P., Beer, C., Ciais, P., Harper, A., Jones, C., Murray-Tortarolo, G.,
676 Papale, D., Parazoo, N. C., & Peylin, P. (2015). Spatiotemporal patterns of terrestrial gross
677 primary production: A review. *Reviews of Geophysics*, 53(3), 785–818.
- 678 Anderegg, W. R., Trugman, A. T., Badgley, G., Anderson, C. M., Bartuska, A., Ciais, P.,
679 Cullenward, D., Field, C. B., Freeman, J., & Goetz, S. J. (2020). Climate-driven risks to the
680 climate mitigation potential of forests. *Science*, 368(6497).
- 681 Arneeth, A., Sitch, S., Pongratz, J., Stocker, B. D., Ciais, P., Poulter, B., Bayer, A. D., Bondeau,
682 A., Calle, L., Chini, L. P., Gasser, T., Fader, M., Friedlingstein, P., Kato, E., Li, W., Lindeskog,
683 M., Nabel, J. E. M. S., Pugh, T. A. M., Robertson, E., ... Zaehle, S. (2017). Historical carbon
684 dioxide emissions caused by land-use changes are possibly larger than assumed. *Nature*
685 *Geoscience*, 10(2), 79–84. <https://doi.org/10.1038/ngeo2882>
- 686 Bajželj, B., Richards, K. S., Allwood, J. M., Smith, P., Dennis, J. S., Curmi, E., & Gilligan, C. A.
687 (2014). Importance of food-demand management for climate mitigation. *Nature Climate*
688 *Change*, 4(10), 924–929.
- 689 Barraclough, S. L. (2013). *Agricultural expansion and tropical deforestation: International*
690 *trade, poverty and land use*. Routledge.

691 Bastos, A., O’Sullivan, M., Ciais, P., Makowski, D., Sitch, S., Friedlingstein, P., Chevallier, F.,
692 Rödenbeck, C., Pongratz, J., & Lujckx, I. T. (2020). Sources of uncertainty in regional and global
693 terrestrial CO₂ exchange estimates. *Global Biogeochemical Cycles*, 34(2), e2019GB006393.

694 Beer, C., Reichstein, M., Tomelleri, E., Ciais, P., Jung, M., Carvalhais, N., Rödenbeck, C.,
695 Arain, M. A., Baldocchi, D., & Bonan, G. B. (2010). Terrestrial gross carbon dioxide uptake:
696 Global distribution and covariation with climate. *Science*, 329(5993), 834–838.

697 Berdanier, A. B., & Clark, J. S. (2016). Multiyear drought-induced morbidity preceding tree
698 death in southeastern US forests. *Ecological Applications*, 26(1), 17–23.

699 Chapin, F. S., Woodwell, G. M., Randerson, J. T., Rastetter, E. B., Lovett, G. M., Baldocchi, D.
700 D., Clark, D. A., Harmon, M. E., Schimel, D. S., & Valentini, R. (2006). Reconciling carbon-
701 cycle concepts, terminology, and methods. *Ecosystems*, 9(7), 1041–1050.

702 Chen, J., Chen, J., Liao, A., Cao, X., Chen, L., Chen, X., He, C., Han, G., Peng, S., & Lu, M.
703 (2015). Global land cover mapping at 30 m resolution: A POK-based operational approach.
704 *ISPRS Journal of Photogrammetry and Remote Sensing*, 103, 7–27.

705 Chen, S., Zhang, Y., Wu, Q., Liu, S., Song, C., Xiao, J., Band, L. E., & Vose, J. M. (2021).
706 Vegetation structural change and CO₂ fertilization more than offset gross primary production
707 decline caused by reduced solar radiation in China. *Agricultural and Forest Meteorology*, 296,
708 108207. <https://doi.org/10.1016/j.agrformet.2020.108207>

709 Coulston, J. W., Reams, G. A., Wear, D. N., & Brewer, C. K. (2014). An analysis of forest land
710 use, forest land cover and change at policy-relevant scales. *Forestry*, 87(2), 267–276.

711 Coulston, J. W., Wear, D. N., & Vose, J. M. (2015). Complex forest dynamics indicate potential
712 for slowing carbon accumulation in the southeastern United States. *Scientific Reports*, 5, 8002.

713 Curtis, P. G., Slay, C. M., Harris, N. L., Tyukavina, A., & Hansen, M. C. (2018). Classifying
714 drivers of global forest loss. *Science*, 361(6407), 1108–1111.
715 <https://doi.org/10.1126/science.aau3445>

716 d’Amour, C. B., Reitsma, F., Baiocchi, G., Barthel, S., Güneralp, B., Erb, K.-H., Haberl, H.,
717 Creutzig, F., & Seto, K. C. (2017). Future urban land expansion and implications for global
718 croplands. *Proceedings of the National Academy of Sciences*, 114(34), 8939–8944.

719 Danielson, J. J., & Gesch, D. B. (2011). *Global multi-resolution terrain elevation data 2010*
720 *(GMTED2010)*. US Department of the Interior, US Geological Survey.

721 Didan, K., Munoz, A. B., Solano, R., & Huete, A. (2015). MODIS vegetation index user’s guide
722 (MOD13 series). *University of Arizona: Vegetation Index and Phenology Lab*.

723 Domke, G. M., Oswalt, S. N., Walters, B. F., & Morin, R. S. (2020). Tree planting has the
724 potential to increase carbon sequestration capacity of forests in the United States. *Proceedings of*
725 *the National Academy of Sciences*, 117(40), 24649–24651.

726 Erb, K.-H., Kastner, T., Luyssaert, S., Houghton, R. A., Kuemmerle, T., Olofsson, P., & Haberl,
727 H. (2013). Bias in the attribution of forest carbon sinks. *Nature Climate Change*, 3(10), 854–856.
728 <https://doi.org/10.1038/nclimate2004>

729 ESA. (2017). *Land cover CCI product user guide version 2*.

730 Falkowski, P., Scholes, R. J., Boyle, E. E. A., Canadell, J., Canfield, D., Elser, J., Gruber, N.,
731 Hibbard, K., Högberg, P., & Linder, S. (2000). The global carbon cycle: A test of our knowledge
732 of earth as a system. *Science*, *290*(5490), 291–296.

733 Fargione, J. E., Bassett, S., Boucher, T., Bridgham, S. D., Conant, R. T., Cook-Patton, S. C.,
734 Ellis, P. W., Falcucci, A., Fourqurean, J. W., & Gopalakrishna, T. (2018). Natural climate
735 solutions for the United States. *Science Advances*, *4*(11), eaat1869.

736 Foley, J. A. (2005). Global Consequences of Land Use. *Science*, *309*(5734), 570–574.
737 <https://doi.org/10.1126/science.1111772>

738 Friedlingstein, P., Jones, M., O’sullivan, M., Andrew, R., Hauck, J., Peters, G., Peters, W.,
739 Pongratz, J., Sitch, S., & Le Quéré, C. (2019). Global carbon budget 2019. *Earth System Science*
740 *Data*, *11*(4), 1783–1838.

741 Frohking, S., Palace, M. W., Clark, D. B., Chambers, J. Q., Shugart, H. H., & Hurtt, G. C. (2009).
742 Forest disturbance and recovery: A general review in the context of spaceborne remote sensing
743 of impacts on aboveground biomass and canopy structure. *Journal of Geophysical Research:*
744 *Biogeosciences*, *114*(G2).

745 Fry, J. A., Coan, M. J., Homer, C. G., Meyer, D. K., & Wickham, J. D. (2008). Completion of
746 the National Land Cover Database (NLCD) 1992–2001 land cover change retrofit product. *US*
747 *Geological Survey Open-File Report*, *1379*, 18.

748 Gorelick, N., Hancher, M., Dixon, M., Ilyushchenko, S., Thau, D., & Moore, R. (2017). Google
749 Earth Engine: Planetary-scale geospatial analysis for everyone. *Remote Sensing of Environment*,
750 *202*, 18–27.

751 Griscom, B. W., Adams, J., Ellis, P. W., Houghton, R. A., Lomax, G., Miteva, D. A.,
752 Schlesinger, W. H., Shoch, D., Siikamäki, J. V., & Smith, P. (2017). Natural climate solutions.
753 *Proceedings of the National Academy of Sciences*, *114*(44), 11645–11650.

754 Guan, X., Shen, H., Li, X., Gan, W., & Zhang, L. (2019). A long-term and comprehensive
755 assessment of the urbanization-induced impacts on vegetation net primary productivity. *Science*
756 *of The Total Environment*, *669*, 342–352.

757 Hansen, M. C., Potapov, P. V., Moore, R., Hancher, M., Turubanova, S. A., Tyukavina, A.,
758 Thau, D., Stehman, S. V., Goetz, S. J., & Loveland, T. R. (2013). High-resolution global maps of
759 21st-century forest cover change. *Science*, *342*(6160), 850–853.

760 Hansis, E., Davis, S. J., & Pongratz, J. (2015). Relevance of methodological choices for
761 accounting of land use change carbon fluxes. *Global Biogeochemical Cycles*, *29*(8), 1230–1246.
762 <https://doi.org/10.1002/2014GB004997>

763 Harris, N. L., Hagen, S. C., Saatchi, S. S., Pearson, T. R. H., Woodall, C. W., Domke, G. M.,
764 Braswell, B. H., Walters, B. F., Brown, S., Salas, W., Fore, A., & Yu, Y. (2016). Attribution of
765 net carbon change by disturbance type across forest lands of the conterminous United States.
766 *Carbon Balance and Management*, *11*(1), 24. <https://doi.org/10.1186/s13021-016-0066-5>

767 Harris, Nancy L., Gibbs, D. A., Baccini, A., Birdsey, R. A., de Bruin, S., Farina, M., Fatoyinbo,
768 L., Hansen, M. C., Herold, M., Houghton, R. A., Potapov, P. V., Suarez, D. R., Roman-Cuesta,
769 R. M., Saatchi, S. S., Slay, C. M., Turubanova, S. A., & Tyukavina, A. (2021). Global maps of
770 twenty-first century forest carbon fluxes. *Nature Climate Change*, *11*(3), 234–240.
771 <https://doi.org/10.1038/s41558-020-00976-6>

772 Homer, C., Dewitz, J., Jin, S., Xian, G., Costello, C., Danielson, P., Gass, L., Funk, M.,
773 Wickham, J., Stehman, S., Auch, R., & Riitters, K. (2020). Conterminous United States land
774 cover change patterns 2001–2016 from the 2016 National Land Cover Database. *ISPRS Journal*
775 *of Photogrammetry and Remote Sensing*, *162*, 184–199.
776 <https://doi.org/10.1016/j.isprsjprs.2020.02.019>

777 Houghton, R. A., House, J. I., Pongratz, J., van der Werf, G. R., DeFries, R. S., Hansen, M. C.,
778 Le Quéré, C., & Ramankutty, N. (2012). Carbon emissions from land use and land-cover change.
779 *Biogeosciences*, *9*(12), 5125–5142. <https://doi.org/10.5194/bg-9-5125-2012>

780 Howard, J. L., & Liang, S. (2019). US timber production, trade, consumption, and price
781 statistics, 1965-2017. *Res. Pap. FPL-RP-701. Madison, WI: US Department of Agriculture,*
782 *Forest Service, Forest Products Laboratory: 1-106., 701, 1–106.*

783 Hurtt, G., Chini, L., Sahajpal, R., Froking, S., Bodirsky, B. L., Calvin, K., Doelman, J., Fisk, J.,
784 Fujimori, S., & Goldewijk, K. K. (2017). *Harmonization of global land use scenarios (LUH2):*
785 *Historical v2. 1h. Earth System Grid Federation.*

786 Jin, S., Homer, C., Yang, L., Danielson, P., Dewitz, J., Li, C., Zhu, Z., Xian, G., & Howard, D.
787 (2019). Overall Methodology Design for the United States National Land Cover Database 2016
788 Products. *Remote Sensing*, *11*(24), 2971. <https://doi.org/10.3390/rs11242971>

789 Klein Goldewijk, K., Beusen, A., Doelman, J., & Stehfest, E. (2017). Anthropogenic land use
790 estimates for the Holocene – HYDE 3.2. *Earth System Science Data*, *9*(2), 927–953.
791 <https://doi.org/10.5194/essd-9-927-2017>

792 Lambin, E. F., Turner, B. L., Geist, H. J., Agbola, S. B., Angelsen, A., Bruce, J. W., Coomes, O.
793 T., Dirzo, R., Fischer, G., & Folke, C. (2001). The causes of land-use and land-cover change:
794 Moving beyond the myths. *Global Environmental Change*, *11*(4), 261–269.

795 Lark, T. J., Meghan Salmon, J., & Gibbs, H. K. (2015). Cropland expansion outpaces
796 agricultural and biofuel policies in the United States. *Environmental Research Letters*, *10*(4),
797 044003. <https://doi.org/10.1088/1748-9326/10/4/044003>

798 Lark, T. J., Spawn, S. A., Bougie, M., & Gibbs, H. K. (2020). Cropland expansion in the United
799 States produces marginal yields at high costs to wildlife. *Nature Communications*, *11*(1), 4295.
800 <https://doi.org/10.1038/s41467-020-18045-z>

801 Le Quéré, C., Andrew, R. M., Friedlingstein, P., Sitch, S., Hauck, J., Pongratz, J., Pickers, P. A.,
802 Korsbakken, J. I., Peters, G. P., & Canadell, J. G. (2018). Global carbon budget 2018. *Earth*
803 *System Science Data*, *10*(4), 2141–2194.

804 Li, C., Sun, G., Cohen, E., Zhang, Y., Xiao, J., McNulty, S. G., & Meentemeyer, R. K. (2020).
805 Modeling the impacts of urbanization on watershed-scale gross primary productivity and
806 tradeoffs with water yield across the conterminous United States. *Journal of Hydrology*, *583*,
807 124581.

808 Li, W., MacBean, N., Ciais, P., Defourny, P., Lamarche, C., Bontemps, S., Houghton, R. A., &
809 Peng, S. (2018). Gross and net land cover changes in the main plant functional types derived
810 from the annual ESA CCI land cover maps (1992–2015). *Earth System Science Data*, *10*(1),
811 219–234. <https://doi.org/10.5194/essd-10-219-2018>

812 Licker, R., Johnston, M., Foley, J. A., Barford, C., Kucharik, C. J., Monfreda, C., & Ramankutty,
813 N. (2010). Mind the gap: How do climate and agricultural management explain the ‘yield gap’ of
814 croplands around the world? *Global Ecology and Biogeography*, *19*(6), 769–782.

815 Liu, J., Sleeter, B. M., Zhu, Z., Loveland, T. R., Sohl, T., Howard, S. M., Key, C. H., Hawbaker,
816 T., Liu, S., Reed, B., Cochrane, M. A., Heath, L. S., Jiang, H., Price, D. T., Chen, J. M., Zhou,
817 D., Bliss, N. B., Wilson, T., Sherba, J., ... Poulter, B. (2020). Critical land change information
818 enhances the understanding of carbon balance in the United States. *Global Change Biology*,
819 *26*(7), 3920–3929. <https://doi.org/10.1111/gcb.15079>

820 Liu, X., Pei, F., Wen, Y., Li, X., Wang, S., Wu, C., Cai, Y., Wu, J., Chen, J., & Feng, K. (2019).
821 Global urban expansion offsets climate-driven increases in terrestrial net primary productivity.
822 *Nature Communications*, *10*(1), 1–8.

823 Noormets, A., Epron, D., Domec, J. C., McNulty, S. G., Fox, T., Sun, G., & King, J. S. (2015).
824 Effects of forest management on productivity and carbon sequestration: A review and
825 hypothesis. *Forest Ecology and Management*, *355*, 124–140.
826 <https://doi.org/10.1016/j.foreco.2015.05.019>

827 Park Williams, A., Cook, B. I., Smerdon, J. E., Bishop, D. A., Seager, R., & Mankin, J. S.
828 (2017). The 2016 southeastern US drought: An extreme departure from centennial wetting and
829 cooling. *Journal of Geophysical Research: Atmospheres*, *122*(20), 10,888–10,905.

830 Pendrill, F., Persson, U. M., Godar, J., Kastner, T., Moran, D., Schmidt, S., & Wood, R. (2019).
831 Agricultural and forestry trade drives large share of tropical deforestation emissions. *Global*
832 *Environmental Change*, *56*, 1–10.

833 Piao, S., Wang, X., Wang, K., Li, X., Bastos, A., Canadell, J. G., Ciais, P., Friedlingstein, P., &
834 Sitch, S. (2020). Interannual variation of terrestrial carbon cycle: Issues and perspectives. *Global*
835 *Change Biology*, 26(1), 300–318.

836 Pielke, R. A. (2005). Land use and climate change. *Science*, 310(5754), 1625–1626.

837 Pongratz, J., Reick, C. H., Houghton, R. A., & House, J. I. (2014). Terminology as a key
838 uncertainty in net land use and land cover change carbon flux estimates. *Earth System Dynamics*,
839 5(1), 177–195. <https://doi.org/10.5194/esd-5-177-2014>

840 Roe, S., Streck, C., Obersteiner, M., Frank, S., Griscom, B., Drouet, L., Fricko, O., Gusti, M.,
841 Harris, N., & Hasegawa, T. (2019). Contribution of the land sector to a 1.5 C world. *Nature*
842 *Climate Change*, 1–12.

843 Rogelj, J., Den Elzen, M., Höhne, N., Fransen, T., Fekete, H., Winkler, H., Schaeffer, R., Sha, F.,
844 Riahi, K., & Meinshausen, M. (2016). Paris Agreement climate proposals need a boost to keep
845 warming well below 2 C. *Nature*, 534(7609), 631–639.

846 Sims, D. A., Rahman, A. F., Cordova, V. D., Baldocchi, D. D., Flanagan, L. B., Goldstein, A. H.,
847 Hollinger, D. Y., Misson, L., Monson, R. K., & Schmid, H. P. (2005). Midday values of gross
848 CO₂ flux and light use efficiency during satellite overpasses can be used to directly estimate
849 eight-day mean flux. *Agricultural and Forest Meteorology*, 131(1–2), 1–12.

850 Sitch, S., Friedlingstein, P., Gruber, N., Jones, S. D., Murray-Tortarolo, G., Ahlström, A.,
851 Doney, S. C., Graven, H., Heinze, C., Huntingford, C., Levis, S., Levy, P. E., Lomas, M.,
852 Poulter, B., Viovy, N., Zaehle, S., Zeng, N., Arneth, A., Bonan, G., ... Myneni, R. (2015).
853 Recent trends and drivers of regional sources and sinks of carbon dioxide. *Biogeosciences*, 12(3),
854 653–679. <https://doi.org/10.5194/bg-12-653-2015>

855 Sitch, Stephen, Friedlingstein, P., Gruber, N., Jones, S. D., Murray-Tortarolo, G., Ahlström, A.,
856 Doney, S. C., Graven, H., Heinze, C., & Huntingford, C. (2015). Recent trends and drivers of
857 regional sources and sinks of carbon dioxide. *Biogeosciences*, *12*(3), 653–679.

858 Sleeter, B. M., Sohl, T. L., Loveland, T. R., Auch, R. F., Acevedo, W., Drummond, M. A.,
859 Sayler, K. L., & Stehman, S. V. (2013). Land-cover change in the conterminous United States
860 from 1973 to 2000. *Global Environmental Change*, *23*(4), 733–748.
861 <https://doi.org/10.1016/j.gloenvcha.2013.03.006>

862 Song, C., Chen, J. M., Hwang, T., Gonsamo, A., Croft, H., Zhang, Q., Dannenberg, M., Zhang,
863 Y., Hakkenberg, C., & Li, J. (2015). Ecological characterization of vegetation using multisensor
864 remote sensing in the solar reflective spectrum. *Remote Sensing Handbook*, *2*, 533–575.

865 Sulla-Menashe, D., Gray, J. M., Abercrombie, S. P., & Friedl, M. A. (2019). Hierarchical
866 mapping of annual global land cover 2001 to present: The MODIS Collection 6 Land Cover
867 product. *Remote Sensing of Environment*, *222*, 183–194.

868 Sun, Z., Wang, X., Yamamoto, H., Tani, H., Zhong, G., Yin, S., & Guo, E. (2018). Spatial
869 pattern of GPP variations in terrestrial ecosystems and its drivers: Climatic factors, CO₂
870 concentration and land-cover change, 1982–2015. *Ecological Informatics*, *46*, 156–165.

871 Tamiminia, H., Salehi, B., Mahdianpari, M., Quackenbush, L., Adeli, S., & Brisco, B. (2020).
872 Google Earth Engine for geo-big data applications: A meta-analysis and systematic review.
873 *ISPRS Journal of Photogrammetry and Remote Sensing*, *164*, 152–170.

874 Thornton, P. E., Thornton, M. M., Mayer, B. W., Wei, Y., Devarakonda, R. S., Vose, R. S., &
875 Cook, R. B. (2017). *Daymet: Daily Surface Weather Data on a 1-km Grid for North America*,
876 *Version 3 ORNL DAAC Oak Ridge Tenn. USA.*

877 van Vliet, J., Eitelberg, D. A., & Verburg, P. H. (2017). A global analysis of land take in
878 cropland areas and production displacement from urbanization. *Global Environmental Change*,
879 *43*, 107–115.

880 Wang, J. A., Sulla-Menashe, D., Woodcock, C. E., Sonnentag, O., Keeling, R. F., & Friedl, M.
881 A. (2020). Extensive land cover change across Arctic–Boreal Northwestern North America from
882 disturbance and climate forcing. *Global Change Biology*, *26*(2), 807–822.
883 <https://doi.org/10.1111/gcb.14804>

884 Wear, D. N., & Greis, J. G. (2002). Southern forest resource assessment: Summary of findings.
885 *Journal of Forestry*, *100*(7), 6–14.

886 Williams, A. P., Allen, C. D., Millar, C. I., Swetnam, T. W., Michaelsen, J., Still, C. J., &
887 Leavitt, S. W. (2010). Forest responses to increasing aridity and warmth in the southwestern
888 United States. *Proceedings of the National Academy of Sciences*, *107*(50), 21289–21294.

889 Wolf, J., West, T. O., Le Page, Y., Kyle, G. P., Zhang, X., Collatz, G. J., & Imhoff, M. L.
890 (2015). Biogenic carbon fluxes from global agricultural production and consumption. *Global*
891 *Biogeochemical Cycles*, *29*(10), 1617–1639.

892 Woodbury, P. B., Smith, J. E., & Heath, L. S. (2007). Carbon sequestration in the US forest
893 sector from 1990 to 2010. *Forest Ecology and Management*, *241*(1–3), 14–27.

894 Wright, C. K., & Wimberly, M. C. (2013). Recent land use change in the Western Corn Belt
895 threatens grasslands and wetlands. *Proceedings of the National Academy of Sciences*, *110*(10),
896 4134–4139. <https://doi.org/10.1073/pnas.1215404110>

897 Yang, L., Jin, S., Danielson, P., Homer, C., Gass, L., Bender, S. M., Case, A., Costello, C.,
898 Dewitz, J., & Fry, J. (2018). A new generation of the United States National Land Cover
899 Database: Requirements, research priorities, design, and implementation strategies. *ISPRS*
900 *Journal of Photogrammetry and Remote Sensing*, *146*, 108–123.

901 Yu, Z., & Lu, C. (2018). Historical cropland expansion and abandonment in the continental U.S.
902 during 1850 to 2016. *Global Ecology and Biogeography*, *27*(3), 322–333.
903 <https://doi.org/10.1111/geb.12697>

904 Yu, Z., Lu, C., Tian, H., & Canadell, J. G. (2019). Largely underestimated carbon emission from
905 land use and land cover change in the conterminous United States. *Global Change Biology*,
906 *25*(11), 3741–3752. <https://doi.org/10.1111/gcb.14768>

907 Zhang, Y., Song, C., Band, L. E., & Sun, G. (2019). No proportional increase of terrestrial gross
908 carbon sequestration from the greening Earth. *Journal of Geophysical Research: Biogeosciences*,
909 *124*(8), 2540–2553.

910 Zhang, Y., Song, C., Band, L. E., Sun, G., & Li, J. (2017). Reanalysis of global terrestrial
911 vegetation trends from MODIS products: Browning or greening? *Remote Sensing of*
912 *Environment*, *191*, 145–155.

913 Zhang, Y., Song, C., Sun, G., Band, L. E., McNulty, S., Noormets, A., Zhang, Q., & Zhang, Z.
914 (2016). Development of a coupled carbon and water model for estimating global gross primary
915 productivity and evapotranspiration based on eddy flux and remote sensing data. *Agricultural*
916 *and Forest Meteorology*, *223*, 116–131.

917 Zhang, Y., Song, C., Zhang, K., Cheng, X., Band, L. E., & Zhang, Q. (2014). Effects of land
918 use/land cover and climate changes on terrestrial net primary productivity in the Yangtze River

919 Basin, China, from 2001 to 2010. *Journal of Geophysical Research: Biogeosciences*, 119(6),

920 1092–1109.

921